Pharmacy   Health Sciences

2024

Potentiometric detection of apomorphine in human plasma using a 3D printed sensor

Manar Elhassan
The British University in Egypt

Dalton Glasco
a Department of Chemistry, Washington State University, Pullman, WA, 99163, USA

Anjaiah Sheelam
Department of Chemistry, Washington State University, Pullman, WA, 99163, USA

amr mahmoud
Cairo University

Maha Hegazy
Cairo University

See next page for additional authors

Recommended Citation

Authors

Manar Elhassan, Dalton Glasco, Anjaiah Sheelam, amr mahmoud, Maha Hegazy, Shereen Mowaka, and Jeffrey Bell

Potentiometric detection of apomorphine in human plasma using a 3D printed sensor

Manar M. Elhassan [a,b], Dalton L. Glasco [a], Anjaiah Sheelam [a], Amr M. Mahmoud [c], Maha A. Hegazy [c,**], Shereen Mowaka [b,d], Jeffrey G. Bell [a,*]

[a] *Department of Chemistry, Washington State University, Pullman, WA, 99163, USA*
[b] *Pharmaceutical Analytical Chemistry Department, Faculty of Pharmacy, The British University in Egypt, El-Sherouk City, 11837, Egypt*
[c] *Analytical Chemistry Department, Faculty of Pharmacy, Cairo University, Kasr El Aini, Cairo, 11562, Egypt*
[d] *Analytical Chemistry Department, Faculty of Pharmacy, Helwan University, Ein Helwan, Cairo, Egypt*

A B S T R A C T

Apomorphine is a dopamine agonist that is used for the management of Parkinson's disease and has been proven to effectively decrease the off-time duration, where the symptoms recur, in Parkinson's disease patients. This paper describes the design and fabrication of the first potentiometric sensor for the determination of apomorphine in bulk and human plasma samples. The fabrication protocol involves stereolithographic 3D printing, which is a unique tool for the rapid fabrication of low-cost sensors. The solid-contact apomorphine ion-selective electrode combines a carbon-mesh/thermoplastic composite as the ion-to-electron transducer and a 3D printed ion-selective membrane, doped with the ionophore calix[6]arene. The sensor selectively measures apomorphine in the presence of other biologically present cations – sodium, potassium, magnesium, and calcium – as well as the commonly prescribed Parkinson's pharmaceutical, levodopa (L-Dopa). The sensor demonstrated a linear, Nernstian response, with a slope of 58.8 mV/decade over the range of 5.0 mM–9.8 μM, which covers the biologically (and pharmaceutically) relevant ranges, with a limit of detection of 2.51 μM. Moreover, the apomorphine sensor exhibited good stability (minimal drift of just 188 μV/hour over 10 h) and a shelf-life of almost 4 weeks. Experiments performed in the presence of albumin, the main plasma protein to which apomorphine binds, demonstrate that the sensor responds selectively to free-apomorphine (i.e., not bound or complexed forms). The utility of the sensor was confirmed through the successful determination of apomorphine in spiked human plasma samples.

1. Introduction

Parkinson's disease is an intricate, progressive neurodegenerative condition that is believed to have multiple etiology due to the interaction of hereditary and environmental variables (Simon et al., 2020). The three motor symptoms that have historically been associated with Parkinson's disease are tremor, stiffness, and bradykinesia, with postural instability frequently developing as the condition worsens. However, there are several non-motor symptoms (e.g., rapid eye movement sleep disorders, constipation, and hyposmia) linked to Parkinson's disease as well, which may appear years or even decades before the motor symptoms do (Kouli et al., 2018). More than 10 million people globally suffer from Parkinson's disease which makes it the second most common

neurodegenerative condition behind Alzheimer's Disease (Mhyre et al., 2012). Regarding healthcare costs, Parkinson's disease is predicted to cost the United States alone over $52 billion annually in direct and indirect expenses, including medical care, social security payments and lost income (Yang et al., 2020).

Apomorphine (APO), (9R)-10-methyl-10-azatetracyclo[7.7.1.0^{2,7}.0^{13,17}]heptadeca-1(16),2(7),3,5,13(17),14-hexaene-3,4-diol, is a dopamine agonist that is used for the management of Parkinson's disease. Its structure, which consists of a tetracycline aporphine ring as shown in Fig. 1, is what gives it the lipophilicity and its affinity for dopaminergic receptors. APO functions as a strong dopamine receptor agonist with a broad spectrum on all D1-and D2-like receptors because of its catechol moiety. Therefore, comparatively to other oral dopamine

---

agonists, APO's method of action is more similar to that of dopamine or its precursor levodopa (Carbone et al., 2019). Studies proved the efficacy of APO in decreasing the off-time duration, where the motor symptoms recur, in Parkinson's disease patients. Additionally, it has been demonstrated that APO helps these individuals' neuropsychiatric issues and other non-motor functions (Carbone et al., 2019; Gaire et al., 2021; Isaacson et al., 2017; Katzenschlager et al., 2018). Unfortunately, APO has many side effects such as nausea, vomiting and hypotension. Additionally, hematologic side effects such as autoimmune hemolytic anemia is another complication of APO therapy making reliable monitoring extremely important during long-term treatment with APO (Carbone et al., 2019).

APO could be delivered by two common ways of administration: intermittent subcutaneous injection or intravenous infusion. Several factors should be considered to determine which way is suitable for the patient. APO injections are usually initiated in a regulated setting in a specialized clinic where the patient can be observed. After the first dose, there are two options to titrate the dose: i) waiting for another off episode to occur and then increase the dose of APO or ii) administering a second dose of APO after 1 h and then every hour after that, increasing the dose by 1 mg each time while recording the motor response. The first option is time consuming and may not allow determination of the effective dose in the same day, but it identifies an accurate dose. While for the second option, which is more practical, this frequency of administration will allow the accumulation of APO in the blood such that the dose will not be identified as precisely as the first option (Bhidayasiri et al., 2015). Therefore, if the blood level could be correlated to the efficacy of APO in controlling the off episodes, this would save time and would help patients to have more controlled off episodes. Many studies were carried out to assess the efficacy of APO for Parkinsonism and correlate the dose with the duration of off periods or the improvement in the motor scores (Esteban Muñoz et al., 1997; Hattori et al., 2014; Ostergaard et al., 1995; Pahwa et al., 2007) but, to the best of our

knowledge, no studies were performed to correlate the blood levels with efficacy.

APO has previously been detected using different analytical methods like high-performance liquid chromatography (HPLC) (Bolner et al., 1997; Dong and Zhang, 2005; Sam et al., 1994; Smith and Humphrey, 1981), surface enhanced Raman spectroscopy (Lucotti et al., 2012; Zanchi et al., 2015) and electrochemical methods (Cheng and Sun, 2001; Cheng et al., 1979; Garrido et al., 2002; Goud et al., 2022). Although HPLC and Raman spectroscopy are automated and precise methods for the determination of APO, these techniques are benchtop, known to be of high cost, and require well trained personnel and lengthy times to operate and evaluate. Whereas electrochemical methods are known for their advantages because of their simplicity, cost effectiveness, and speed. Electrochemical sensors are powerful tools that are frequently employed in pharmaceutical, environmental, medical, and industrial applications. In pharmaceutical and medical fields, electrochemical sensors were recently employed for the detection of many biologically significant analytes as the biomarkers associated with severe acute respiratory syndrome coronavirus (Karuppaiah et al., 2023) and cholera toxins (Kim et al., 2023).

Although voltammetric or amperometric biosensors make up the great majority of electrochemical biosensors, potentiometric sensors are becoming more and more popular because of their benefits (Walker et al., 2021). Owing to its high selectivity, low detection limits, ease of use, portability and ability to be performed using portable potentiostats, potentiometry or the use of ion-selective electrodes (ISEs) has emerged as an appealing alternative to other analytical techniques. ISEs were successfully used for the detection of many analytes (e.g., fluoride, creatinine and Phenytoin) (Guinovart et al., 2017; Huang et al., 2019; Jansod et al., 2016). An additional advantage of potentiometry is its power efficiency, since during electrochemical process, the potential across an interface between a working electrode and a reference electrode is measured while a very small bias current flows (Ding and Qin,
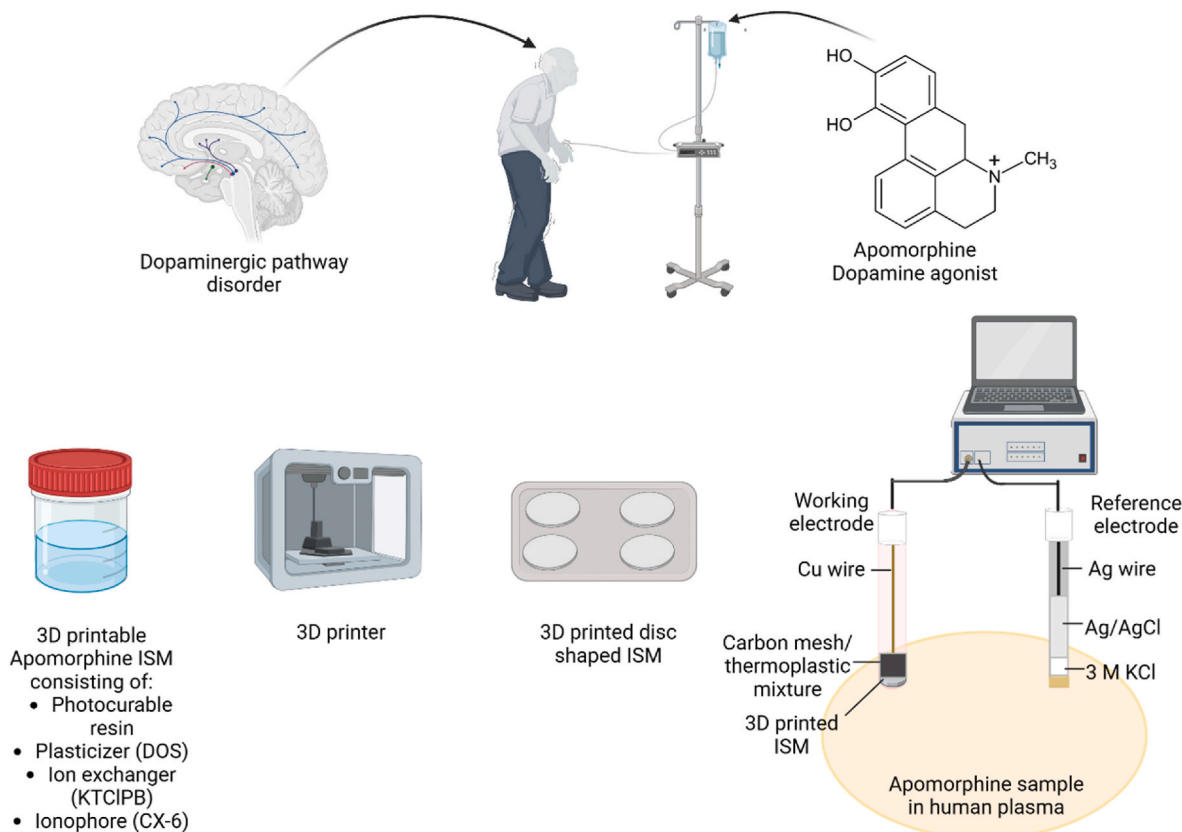

Fig. 1. Schematic representation for 3D printing of APO$^+$ ISM and their translation into solid-contact ISE. *Created with Biorender.com*.

2020; Walker et al., 2021). Furthermore, this negligible current indicates that the technique should be less susceptible to ohmic drop concerns and interferent effects, when compared to voltametric and amperometric sensors (Smith et al., 2020). Lastly, it has been demonstrated that potentiometry is relatively insensitive to electrode size, indicating that miniaturization could be achieved without sacrificing sensitivity (Park et al., 2013). 3D printing is proving to be an incredibly helpful tool in a range of analytical chemistry applications by combining the adaptability of chemistry with recent developments in materials production (Glasco et al., 2022). 3D printing is anticipated to play a pivotal role in revolutionizing healthcare and clinical practice, because it offers the ability to construct personalized devices designed for the individual variations of patient populations (Diment et al., 2017). The development of 3D printable materials with built-in functionality opens up new possibilities for the creation of stimulus-responsive devices (Palmara et al., 2021). The advantages of fabricating ion-selective membranes (ISM) via 3D printing include i) ISMs can be mass produced, ii) have exact control over their shape and size and iii) require less time to fabricate (Glasco et al., 2021). 3D printed ISMs have successfully been applied to the development of ISEs for the selective determination of K^+, Ca^{2+} (Mamaril et al., 2022), bilirubin (an important ionic biomarker of liver health), and benzalkonium (a common preservative in eye drops) (Ho et al., 2022). The strategy used for 3D printing the ISM in this work is stereolithography (SLA). This method uses a photopolymer, which undergoes a chemical reaction when exposed to UV/IR light, changing its physicochemical properties. Due to its excellent surface texture and fastest and highest resolution 3D printers, it carries considerable potential supremacy (Pavan Kalyan and Kumar, 2022).

Due to the increasing need to improve the sensors' sensitivity and selectivity, ionophores, such as macrocyclic chemicals, are added to ISM's composition, as they have exceptional supramolecular recognition capabilities. The structure of the macrocyclic compound and the size of the cavity it forms are crucial considerations when choosing which one to include in the design of the electrochemical sensor (Luo et al., 2019). When compared to other macrocycles, calixarenes have many advantages when used as hosts for the binding of ammonium moieties, as APO, due to excellent accessibility, the ability to modify the inner cavity's size and shape, and the addition of different functional groups to handle almost any ammonium moiety guest selectivity (Späth and König, 2010).

This work represents the first potentiometric sensor for the determination of the cationic form (APO^+). For this, 3D printing technology was used to print the functional component of the ISE; the ion-selective membrane (ISM). These 3D printed ISMs were integrated into 3D printed housings containing a carbon mesh/thermoplastic composite serving as the solid-contact ion-to-electron transducer. The fabricated 3D printed APO^+-ISE (3Dp-APO^+-ISE) displayed selective detection of APO^+ in bulk and human plasma. This sensor will allow the measurement of APO^+ levels in blood thereby facilitating reliable pharmaceutical dosing of APO for more controllable off episodes and better quality of life for Parkinson's disease patients.

2. Experimental

2.1. Chemicals and reagents

Apomorphine ($C_{17}H_{17}NO_2$, $\geq$98.5%), bis-2-ethylhexyl sebacate (DOS, $C_{26}H_{50}O_4$, >97.0%), nitrophenyl octyl ether (NPOE, $C_{14}H_{21}NO_3$, >99.0%), potassium tetrakis(4-chlorophenyl)borate (KTClPB, $C_{24}H_{16}BCl_4K$, >98.0%), Calix[6]arene (CX-6, $C_{42}H_{36}O_6$, 97%), phosphate buffer (1M), potassium chloride (KCl), Hydrochloric acid (HCl, 6.0M), levodopa (L-Dopa, $C_9H_{11}NO_4$) and Bovine Serum Albumin were all purchased from Sigma. Carbon fiber rods were purchased from Aopin. All solutions were prepared using DI water. Photocurable resin base of an acrylate monomer, urethane dimethacrylate, and photoinitiator (Flexible 80A) was purchased from Formlabs. Magnesium

chloride ($MgCl_2$) was purchased from VWR international, USA. Sodium chloride (NaCl) and calcium chloride ($CaCl_2$) were purchased from EMD Millipore, Germany. Carbon mesh (PAN Graphite Felt - 3.1 mm thick) was purchased from Fuel Cell, United States. Human plasma was purchased from Innovative Research Inc. (Michigan, USA).

2.2. Instruments

A 16-channel potentiometer was purchased from Lawson Labs and was utilized for obtaining the electromotive force (*emf*) vs time data for all the fabricated electrodes. For curing the membranes, a 365 nm UV oven was employed and was purchased from Melody Susie. Apera pH meter (PH700) was used to adjust the pH of APO solutions.

2.3. Procedures

2.3.1. Fabrication of the ISM

The ISM was prepared by mixing 94.14% photocurable resin, 3.9% DOS, 1.33% KTClPB and 2:1 mol ratio of KTClPB to CX-6. These components were mixed and stirred then allowed to dissolve overnight to have a final homogenous solution.

2.3.2. CAD and 3D printing

Computer aided design (CAD) files were generated using the software Fusion 360. A CAD file for the ISE housing was designed with a length of 50 mm and an outer diameter of 8 mm (Figure SI1). The sensing end of the housing included a 5 mm diameter channel with a depth of 4 mm. A 1.2 mm diameter channel was embedded through the entire housing. A CAD file for 3D printing APO^+-ISMs was created with a 25 mm by 25 mm square with a thickness of 0.4 mm. Once the CAD files were generated an open-source slicing software was used to prepare 3D print files for each 3D printer. For ISE housings a Form 3 SLA 3D printer (FormLabs Inc.) was used to fabricate the housings. For the ISM a Mars 2 SLA 3D printer (Elegoo Inc.) was used to fabricate each membrane.

2.3.3. Preparation of the solid contact ISE and APO^+ calibration

After generating a CAD file for the ISE housing, the file was uploaded to the slicing software and transferred to the Form 3 3D printer. The file was then printed using Clear V4 (FormLabs Inc.) resin. After printing the housings were rinsed in isopropyl alcohol (IPA) for 15 min and then each channel was cleared thoroughly with compressed air and IPA. After removing excess resin, the housings were placed in a UV oven for 30 min to finish the crosslinking process. A 3D printed APO^+-ISM was also printed and rinsed in IPA for 2 min to remove excess resin.

While the housings were in the UV oven, a carbon mesh paste was created using fibrous carbon mesh mixed with an epoxy (Eclectic Products) at a ratio of 1:2 wt %. After the housings are removed from the UV oven, a 1.2 mm dia copper wire is placed in the ISE housing and then covered with the carbon mesh paste and left for 12 h to dry. After the paste has dried an 8 mm diameter disk of the 3D printed APO^+-ISM is affixed to the ISE housing (containing the carbon mesh paste) and cured for 15 min. The previous steps are captured and shown in Figure SI2. Once cured, the 3Dp-APO^+-ISE is placed in a conditioning solution (10 μM APO^+ in phosphate buffer, pH 4.5) until further use.

For the calibration of APO^+, Ag/AgCl was used as reference electrode, and we started with 10 mLs of a 5.0 mM solution of APO^+ in 0.01 M phosphate buffer of pH 4.5 (made acidic through dropwise addition of 0.1 M HCl). The calibration was then performed using 1:1 dilutions by withdrawing 5 mL of the existing solution and adding 5 mL of the diluting solution (0.01 M phosphate buffer of pH 4.5). The *emf* was recorded during the whole process until there are no more Nernstian response to the change of the concentration.

2.3.4. Water layer test analysis

The *emf* response was recorded for a conditioned 3Dp-APO^+-ISE that was immersed in 1 mM APO^+ at pH 4.5 for 4 h. Next, the electrode was

placed in 1 mM KCl (pH 4.5) for 3 h then in 1 mM APO $^+$ at pH 4.5 for 4 h. The *emf* was recorded continuously and the presence of drift in the *emf* of the ISE while being in 1 mM APO $^+$ for the last 4 h indicates the presence of the water layer (Hambly et al., 2020).

2.3.5. Effect of pH

The effect of pH on the 3Dp-APO$^+$-ISE response was investigated in the pH range (2–10). By adding aliquots of 0.1 M HCl and 0.1 M NaOH solutions to a 0.01 M phosphate buffer, the specific pH was produced. At every pH level, the *emf* signals of two different APO $^+$ concentrations (1.0 mM and 100.0 μM) were measured.

2.3.6. Selectivity studies

The selectivity of the produced electrodes was tested by conditioning them in 10.0 μM APO $^+$ overnight and then the *emf* values were recorded for 1 mM of calcium, magnesium, sodium, potassium, and levodopa. All solutions for selectivity studies were prepared by dissolving the required amount of chemical to make 20 mL of a 1 mM solution of the potentially interfering species in 0.01 M phosphate buffer (pH 4.5). The log selectivity coefficients were calculated for each potential interferent using the following equation:

$$log\ K_{a,x}^{pot} = \frac{Z_a\ (E_x\ -\ E_a)}{59.2} + log\left(\frac{C_a}{C_x^{\left(\frac{Z_a}{Z_x}\right)}}\right) \tag{1}$$

Where, K^{pot} is the selectivity coefficient, E$_x$ is the *emf* response to the analyte, E$_a$ is the *emf* response to the interfering ion, Z$_a$ is the charge of the analyte, Z$_x$ is the charge of the interfering ion, C$_a$ is the concentration of the analyte and C$_x$ is the concentration of the interfering ion.

2.3.7. Application in plasma

The fabricated APO$^+$-ISE was applied toward the determination of APO$^+$ in plasma. 3Dp-APO$^+$-ISE were placed in a beaker with a Ag/AgCl reference electrode and stir bar. The beaker was placed on a stir plate where 5 mL of human plasma was then added to the beaker and stirred. APO$^+$ was then additively spiked in plasma where a 5-point calibration was collected from 35 to 700 μM APO$^+$. After the calibration each 3Dp-APO$^+$-ISE was rinsed and placed in a new beaker with fresh human plasma. Then, three unknown concentrations (50, 169 and 600 μM) representing low, middle and high levels, were spiked by adding 100, 250, and 1000 μL of a 5 mM stock APO solution, and the concentrations were determined using the regression equation.

2.3.8. Stability and Shelf-life

To determine the stability of the 3Dp-APO$^+$-ISE, the *emf* response was recorded for a conditioned electrode that was placed in 100 μM APO$^+$ in phosphate buffer of pH 4.5 and in plasma for 10 h.

A shelf-life analysis was completed for 3Dp-APO$^+$-ISE, where conditioned ISEs were monitored over the course of 32 days. An *emf* response was recorded for each 3Dp-APO$^+$-ISE in a 1 mM APO$^+$ solution at pH 4.5 every 2 days until day 27 where each ISE was then monitored daily until day 32. Between measurements the 3Dp-APO$^+$-ISE were stored at room temperature in a closed cabinet.

2.3.9. Method validation

To ensure that the method is suitable for its intended purpose which is the determination of APO$^+$ in bulk, we validated our method according to the International Council for Harmonization's guidelines (*ICH Harmonized Tripartite Guideline, Validation of Analytical Procedures: Text and Methodology, Q2 (R1), Current step 4 version, Parent guidelines on Methodology,* 1996). Linearity was evaluated by determining ten different concentrations of APO$^+$ in triplicate. A calibration curve was obtained by plotting the *emf* response recorded versus the respective

concentration. Accuracy was assessed by calculating the percentage recovery of three different concentrations of APO$^+$. Precision was tested by determining three different concentrations of APO$^+$ three times on the same day for the intraday precision and on three different days for the interday precision, then calculating the percentage relative standard deviation (%RSD). According to the IUPAC regulations, limit of detection (LOD) was calculated by extrapolating the lines of the Nernstian and non-Nernstian response whereas, limit of quantification (LOQ) is the lowest concentration in the calibration curve which can be determined accurately and precisely (Buck and Lindner, 1994).

3. Results and discussion

3.1. Fabrication and sensing mechanism of the 3Dp-APO$^+$-ISE

The component of the 3Dp-APO$^+$-ISE that is responsible for the sensing of APO$^+$ in solution is the ISM. The membrane consists of a photocurable resin, a plasticizer, an ion exchanger, and an ionophore, which make up the 3D printable Apomorphine ISM cocktail (Fig. 1). The resin is responsible for providing the structural support for the ISM, analogously to polyvinyl chloride (PVC) in PVC-based ISMs. The role of the plasticizer is to improve the solubility of the membrane components and enhance the analyte's mobility within the membrane. By exchanging its potassium ions with the positively charged APO$^+$ ions, the ion exchanger's function is to render the ISM sensitive to positively charged molecules (i.e., permselective). The ionophore, a neutral molecule, endows the ISM with enhanced selectively towards the target analyte, here APO$^+$.

In order to achieve an optimum response towards APO$^+$, we optimized different parameters and compared the electrodes' performance regarding the linear range, limit of detection (LOD), and the slope of the calibration curve which should, under standard conditions, be equal to 59.2 mV, according to Nernst equation (Equation (2)),

$$emf = E^0 + \frac{RT}{zF}\ln a = E^0 + \frac{59.2\ mV}{z}\log c \tag{2}$$

where E^0 is the standard potential, R is the gas constant, T is the temperature, F is Faraday's constant, z is the ion's charge and c is the ion's concentration. Since the phosphate buffer maintains a constant ionic strength in the measuring solutions, we assume a constant activity coefficient for the APO$^+$, and report *emf* vs. concentration.

First, we investigated two different plasticizers (differing in their polarities), DOS and NPOE. Membranes containing DOS produced better Nernstian responses and lower LOD. By varying the amount of DOS in the ISM, it was found that membranes containing 3.9% DOS were optimal with respect to Nernstian response, linear range and the LOD. We then investigated the role of the ionophore by incorporating the calixarenes, as CX-6, Calix[4]arene and Calix[8]arene because they have good accessibility when they act as a host for ammonium moiety and β-cyclodextrin. It was found that CX-6 produced the best results in terms of linear range, LOD and Nernstian response (as CX-6 possesses the most suitable cavity size for APO$^+$ molecule, capable of interacting with the ammonium moiety via electrostatic attraction between the electron rich faces of the aromatic rings of CX-6 and the positive charge of APO$^+$ (Späth and Knig, 2010)). Previous research has shown that the ratio of ion exchanger to ionophore is an important consideration in the fabrication of ISEs, and the ratio of KTClPB: CX-6 (2:1) resulted in better Nernstian responses. Lastly, the concentration (10 μM and 100 μM) and the pH (4, 4.5, 5 and 5.5) of the conditioning solution was optimized. Those pH values were chosen according to the stability and the pKa of APO$^+$, which is equal to 8.92 ("National Center for Biotechnology Information (2023). PubChem Compound Summary for CID 6005, Apomorphine.," n.d.). 10.0 μM APO$^+$ in 0.01 M phosphate buffer of pH 4.5 was the most effective solution due to the relative instability of APO in other pH values (Sam et al., 1994). The results of all membrane

optimizations are summarized in Table SI1. Table SI2 represents a comparison of the analytical performance of the optimized APO$^+$-ISE to other reported methods for apomorphine quantification in terms of linear range and LOD. As previously mentioned, APO has been determined using two different electrochemical approaches. The first one is based on the detection of APO on a Nafion film modified glassy carbon electrode using square-wave voltammetry. Although the LOD (3×10^{-9} M) using this method was lower than the 3Dp-APO$^+$-ISE (2.51×10^{-6} M), the Nafion modified electrode requires expensive reagents and materials, and an accumulation process prior to analysis, making the approach more costly and time-intensive (Cheng and Sun, 2001). In 2022, Gould et al., reported a wearable APO sensor based off voltammetry and amperometry, that relied on a carbon paste and Nafion modified microneedle. This sensor exhibited a sufficient LOD (0.6×10^{-6} M) for quantification of APO in interstitial fluid, although such results need to be correlated to blood levels (Goud et al., 2022).

The optimized ISM composition was found to be 94.14% photocurable resin, 3.9% DOS, 1.33% KTClPB and 2:1 mol ratio of KTClPB to CX-6. Fig. 2A shows a representative *emf* vs. time trace obtained for successive 1:1 dilutions, and as can be seen, upon dilution the resulting *emf* decreases and rapidly becomes stable. Fig. 2B represents the calibration curve of APO$^+$ using the 3Dp-APO$^+$-ISE with a slope of 58.8 mV/Decade. The triangle inset shows the theoretically expected slope (59.2 mV decrease in *emf* upon an order of magnitude change in concentration of APO$^+$).

3.2. Evaluation of solid-contact carbon mesh/thermoplastic

An ideal solid contact ion-to-electron transducer should have the following characteristics in order to produce a stable and reproducible solid contact ISE: i) inherent hydrophobicity, ii) high capacitance to prevent polarization under high exchange current density, iii) reversible

Fig. 2. A. Time series representing the *emf* response to 1:1 dilutions of 5.0 mM APO$^+$ solution. B. Linear response of APO$^+$ in the range of 5.0 mM–9.8 μM with a slope 58.8 mV/Decade.

ion-electron transduction and iv) the absence of undesirable side reactions (Monia Fibbioli et al., 2000; Liu et al., 2021; Nikolskii and Materova, 1985). Therefore, the properties of the solid-contact ion-to-electron transducer, the carbon mesh/thermoplastic composite, which is presented here for the first time in the fabrication of an ISE, was evaluated using surface characterization and electrochemical techniques. Fig. 3A shows an SEM image of the carbon mesh/thermoplastic composite, where the dark features are indicative of the carbon material and the light features are the epoxy. The hydrophobicity of the composite was tested by introducing a drop of water on the surface of a dried and flattened composite, as shown in Fig. 3B. The contact angle was found to be 135° indicating a high hydrophobicity of the mixture (Kumar and Prabhu, 2007). Reported work has demonstrated that enhancing the hydrophobicity of the solid contact ion-to-electron transducer is an efficient means of preventing the formation of an undesirable water layer that can be formed at the interface between the ion-to-electron transducer and the ISM. Even minute transmembrane fluxes of the analyte of interest and interfering ions can change the ionic composition in this water layer, which has a negative impact on the potential stability and reproducibility of ISEs (M. Fibbioli et al., 2000; Liu et al., 2021). To evaluate the presence of a water-layer between the APO$^+$-ISM and carbon mesh/thermoplastic solid-contact composite, we performed the well-known "water layer test". As represented in Fig. 3C, after placing the 3Dp-APO$^+$-ISE first in a solution of 1 mM APO$^+$ (for 4 h), then in a solution of 1 mM KCl (for 3 h) and then back into the 1 mM APO$^+$ solution (for 4 h), negligible drift in the *emf* was observed in the final solution of APO$^+$, therefore, there is no water layer between the carbon mesh/thermoplastic composite layer and the 3D printed ISM. Regarding the second requirement of stable solid-contact ion-to-electron transducers, which is high capacitance, its magnitude is highly dependent on the component used as solid contact in the ISE. Given that the ion-to-electron transduction process creates an asymmetric condition, a high capacitance is necessary to produce a high exchange current and, consequently, a solid contact that is nonpolarizable (Bobacka, 1999). To evaluate the polarization of the fabricated 3Dp-APO$^+$-ISE, we compared it to a glassy carbon electrode. Muti-step chronopotentiometric technique was used for a single cycle at two levels (1.0 and −1.0 nA) for 60 s each. As represented in Fig. 3D, a smaller potential jump is observed for the ISE composed of the carbon mesh/thermoplastic composite when compared to the glassy carbon electrode. These results confirm that the carbon mesh/thermoplastic composite is a viable option in the construction of reliable solid-contact ion-to-electron transducers for potentiometric applications.

3.3. Effect of pH

Since pH not only affects the ionization of APO (and in turn its ability to be sensed potentiometrically) but also its stability, it was a crucial factor to evaluate. At pH higher than 6, the stability of APO is decreased, and a blue solution is produced instead of a clear solution. While at pH higher than 9, a black solution is observed. The instability of APO in alkaline environments has been reported. Photographs of as-prepared APO$^+$ solutions at different pH values are shown in Figure SI3. Fig. 4A shows the influence of pH on the resulting slope obtained for the 3Dp-APO$^+$-ISE at different pHs. Here we see a significantly sub-Nernstian response at pH 2, which increases to approximately 50 mV/decade at a pH of 3. At the operational pH of 4.5, the 3Dp-APO$^+$-ISE responds in a Nernstian fashion before again decreasing as the pH is increased to 6 and 7. The large error bars observed at pH 7 is likely due to the instability of APO$^+$ at that pH as well as incomplete ionization.

3.4. Selectivity and application in plasma

The ISE needs to have adequate selectivity for the target analyte in order to function as a sensor, particularly when the target analyte is frequently found in complex media like plasma. The selection of the
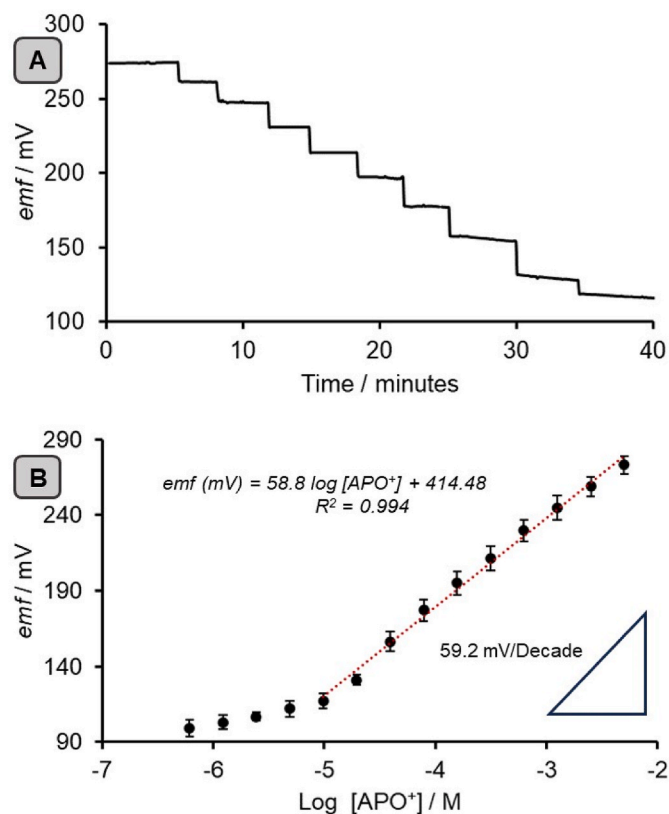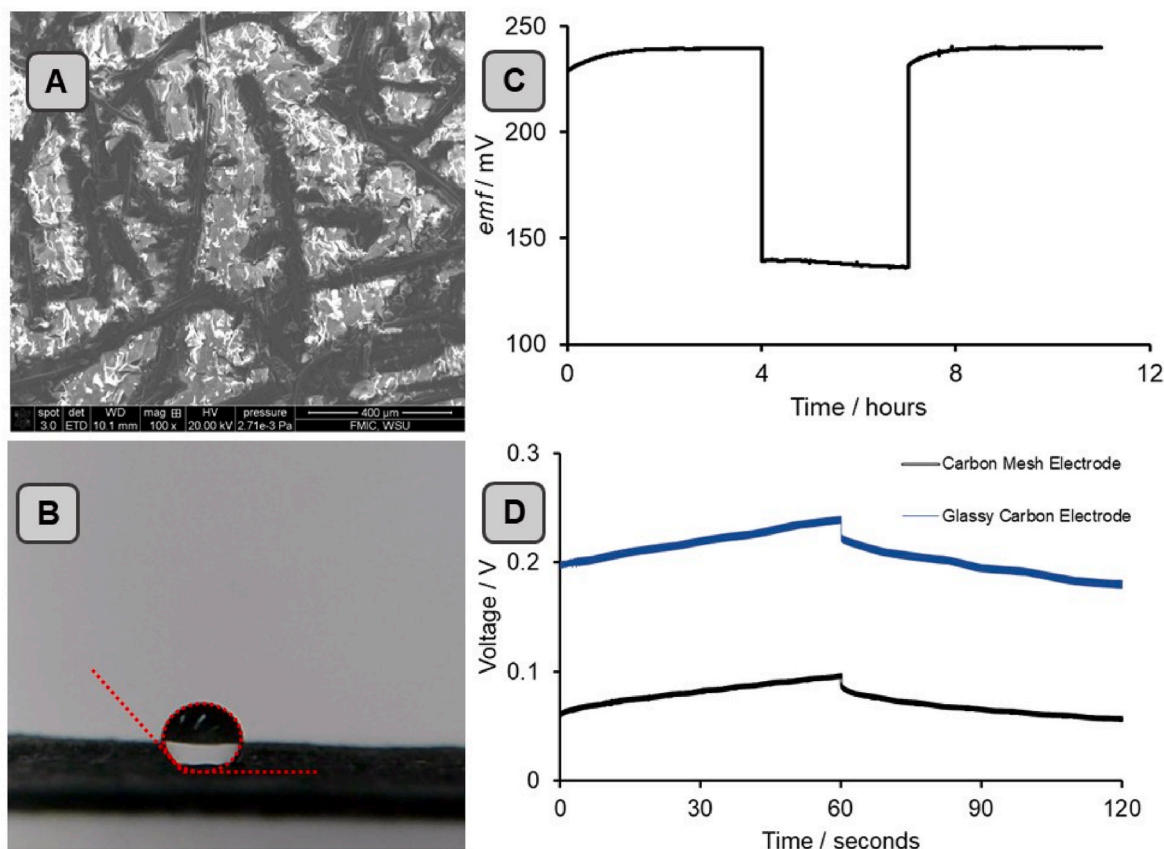
Fig. 3. A. SEM image of Carbon mesh/thermoplastic composite B. Hydrophobicity test for the Carbon mesh/thermoplastic composite. C. Multi-step potentiometry at two levels (1.0 and −1.0 nA) for Carbon mesh/thermoplastic composite and glassy carbon electrodes. D. Water layer test for 3Dp-APO$^+$-ISE immersed in 1 mM APO$^+$ at pH 4.5 for 4 h, then in 1mM KCl for 3 h then back in 1 mM APO$^+$ at pH 4.5 for 4 h.

ionophore to be incorporated in the membrane depends on the expected selectivity to the analyte of interest. Herein, we investigated macrocyclic calixarenes due to their reported selectivity towards quaternary ammonium compounds such as APO (Bell et al., 2018; Michael et al., 2023; Mousavi et al., 2018). Fig. 4B represents the observed *emf* response of the 3Dp-APO$^+$-ISE in 1 mM solutions of Mg^{2+}, Ca^{2+}, Na$^+$, K$^+$ and levodopa (L-Dopa) versus the response for the same concentration of APO$^+$. Although L-Dopa does not display full cationic character at this pH (predominately zwitterionic), L-Dopa is the primary pharmaceutical intervention for patient's with Parkinson's disease, and would be present in their biological fluids. The experimental determined selectivity coefficients were computed using Equation (1) and are shown in Table 1. These results show that the 3Dp-APO$^+$-ISE, incorporating CX-6 as the ionophore, displays great selectivity towards APO$^+$ over other potential cationic interfering species.

As the 3Dp-APO$^+$-ISE is intended to determine APO$^+$ in plasma, an experiment was performed to ensure the ability of the 3Dp-APO$^+$-ISE to detect APO$^+$ in the presence of albumin. As shown in Fig. 4C, first, the 3Dp-APO$^+$-ISE was immersed in a background solution consisting of all the studied interferents at their maximum physiological concentrations. Then, the electrode was placed in 20.0 μM APO$^+$ followed by 200.0 μM APO$^+$. Finally, 200.0 μM APO$^+$ in the presence of 100.0 μM albumin was added. The presence of albumin decreased the *emf* response of APO$^+$ by 5 mV, but it is still detectable indicating that the 3Dp-APO$^+$-ISE can be used for the determination of APO$^+$ in plasma.

After we confirmed the ability of the 3Dp-APO$^+$-ISE to detect free APO$^+$ in the presence of albumin, we applied the method for the determination of APO$^+$ in plasma (Table 2). Fig. 5A represents the *emf* response to five different concentrations of APO$^+$ spiked in plasma in the range of 35.0–700.0 μM with a near Nernstian slope of 52 mV/

decade. This range was chosen as it represents the relevant range in plasma as previously reported (Manson et al., 2001). Three unknown concentrations (50, 169 and 600 μM) representing low, medium and high levels, were spiked, and the concentrations were estimated using the regression equation. The percentage recovery are represented in Table 2.

3.5. Stability, shelf life and validation

One of the characteristics of any good sensor is its stability over time. To evaluate the stability of the 3Dp-APO$^+$-ISE, we measured the evolution of the *emf* over a period of 10 h in 100 μM APO$^+$. The 3Dp-APO$^+$-ISE showed good stability, as represented in Fig. 5B, with a change of 188 μV/hr when in phosphate buffer of pH 4.5 and a change of 688 μV/hr in plasma. The larger deviation in the plasma solution is likely due to biofouling processes such as protein adsorption to the ISM. To determine the lifetime of the 3Dp-APO$^+$-ISE, the *emf* response was recorded for three 3Dp-APO$^+$-ISEs in a 1 mM APO$^+$ solution at pH 4.5 over the course of 32 days. Interestingly, the sensors maintained their effectiveness for 27 days before the observed *emf* response started to decrease. Regarding the validation, Table 3 shows the results of all validation parameters calculated as outlined in the experimental section. The 3Dp-APO$^+$-ISE responded linearly in the range of 9.77 μM to 5.0 mM, with an LOD of 2.51 μM and an LOQ of 9.77 μM. The method was proven to be accurate as the percentage recoveries for the spiked samples were in the accepted range (100 ± 2). Moreover, the precision was also determined to be in the accepted range (%RSD <2). Owing to the rise in the recognition of the importance of sustainability and green chemistry and that most of efforts to make greener analytical methodologies focus on minimizing energy consumption and employing safer or less hazardous solvents
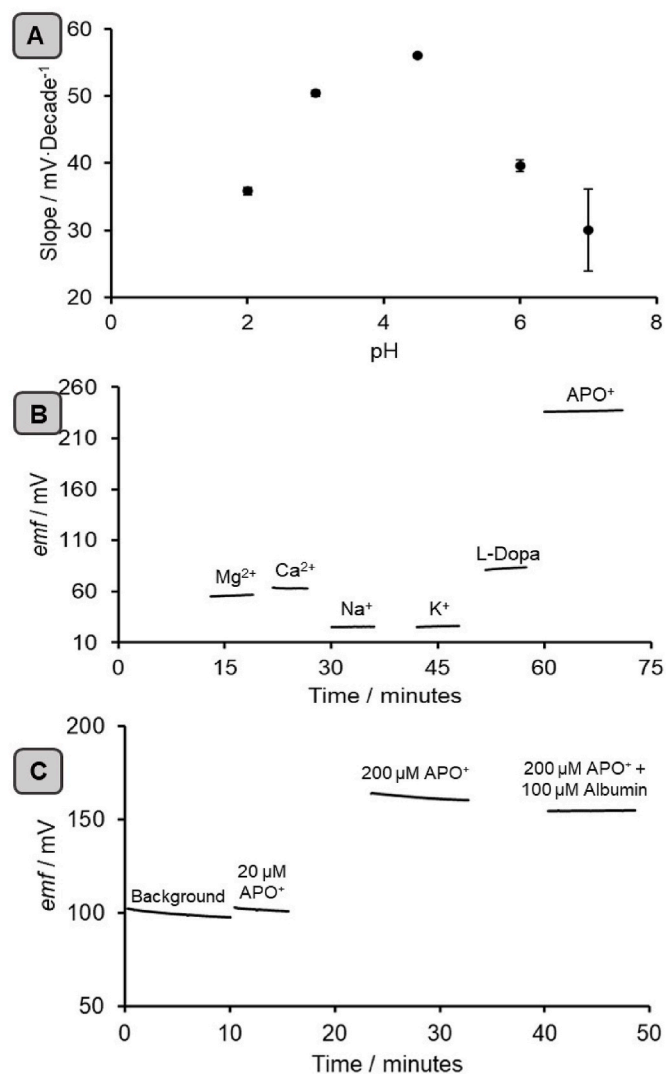
Fig. 4. A. Effect of pH on the *emf* responses of the 3Dp-APO⁺-ISE immersed in 1.0 mM and 100.0 μM APO⁺. B. Selectivity study showing the *emf* readings obtained for 1.0 mM Mg²⁺, Ca²⁺, Na⁺, K⁺, L-dopa and APO ⁺ versus time. C. *emf* responses of the 3Dp-APO⁺-ISE to 20 μM APO⁺, 200 μM APO⁺ and 200 μM APO⁺ in the presence of 100 μM Albumin (all solutions are prepared in a background solution consisting of 145.0 mM Na⁺, 5.50 mM K⁺, 2.70 mM Ca²⁺, 1.10 mM Mg²⁺ and 0.014 mM L-dopa in buffer of pH 4.5).

Table 1
Selectivity coefficients for biologically relevant interfering cations versus APO ⁺ for CX-6 doped ISE.

Interferent	Concentration (M)	Physiological ranges (mM) (Shrimanker and Bhattarai, 2023)	Log k
Magnesium	0.001	0.60 to 1.10	-3.08 ± 0.13
Calcium	0.001	2.20 to 2.70	-3.23 ± 0.16
Sodium	0.001	135.0 to 145.0	-3.64 ± 0.08
Potassium	0.001	3.60 to 5.50	-3.61 ± 0.08
L-Dopa	0.001	0.008 to 0.014 (Kuoppamäki et al., 2009)	-2.66 ± 0.10

(Sajid and Płotka-Wasylka, 2022), we calculated the greenness of this analytical method (i.e., the use of the 3Dp-APO⁺-ISE), Table SI3. Here we see that based on the components of the 3Dp-APO⁺-ISE, its use as an

Table 2
Results of spike recovery analysis in plasma.

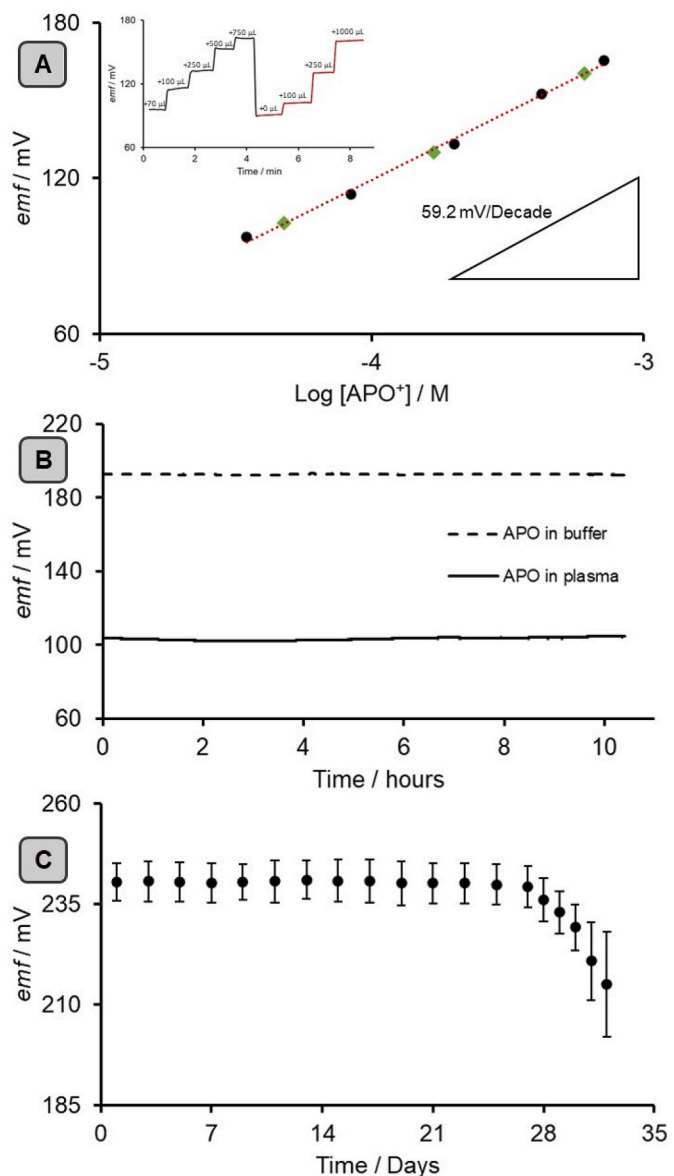| Linear Range/μM	35–700
Low unknown [APO⁺]/μM	50
Recovery [APO⁺]/μM	48 ± 9
% Recovery	96 ± 19
Medium unknown [APO⁺]/μM	169
Recovery [APO⁺]/μM	159 ± 7
% Recovery	94 ± 5
High unknown [APO⁺]/μM	600
Recovery [APO⁺]/μM	610 ± 96
% Recovery	102 ± 16

Fig. 5. A. Calibration curve of APO⁺ in plasma in the concentration range (35.0.0–700.0 μM). Green data points represent unknown APO⁺ samples. B. Stability for 3Dp-APO⁺-ISE immersed 100.0 μM APO⁺ at pH 4.5 for 10 h and 100.0 μM APO⁺ in plasma. C. *emf* responses in 1.0 mM APO ⁺ over a period of 32 days.

analytical tool receives an "Analytical eco-scale" total score of 92, which puts it in the category of an excellent green analytical tool (Gałuszka et al., 2012).

Table 3
Validation parameters for the suggested sensor.

Parameters	Proposed sensor
Regression equation	y = 58.8x + 414.48
Linearity range	9.8 μM–5.0 mM
Correlation coefficient	0.994
Accuracy	99.59 ± 1.57
Intraday precision	1.93
Interday precision	1.96
LOD	2.51 μM
LOQ	9.8 μM

4. Conclusion

In this work, we developed the first potentiometric sensor for the determination of APO^+ and confirmed its utility in bulk and in human plasma. The 3Dp-APO^+-ISE consists of a 3D printed ISM doped with the ionophore calix[6]arene which is affixed to a 3D printed housing containing a carbon mesh/thermoplastic composite as the solid contact material. The 3Dp-APO^+-ISE was found to be selective and able to detect APO^+ over the biologically and pharmaceutically relevant ranges in human plasma. The sensor was stable for approximately 10 h with a minimal drift of just 188 μV/hr without the formation of a water layer. Using 3D printed potentiometric sensors for the determination of APO^+ has several advantages: i) it requires simple equipment for readout, ii) the method is cost effective and rapid, iii) 3D printed ISMs can be easily translated into point-of-care devices owing to the control afforded by 3D printing. Furthermore, 3D printing permits a rapid print/test/iterate/ optimize approach which has the ability to drastically reduce the time required to fabricate reliable sensors. The inherent reproducibility afforded by 3D printing also translates to sensor reproductivity, where device-to-device deviations can be significantly decreased. While 3D printing in the field of potentiometry is still in its infancy, the performance of the 3Dp-APO^+-ISE provides evidence justifying continued research in this area. Miniaturization and implementation into hand-held devices that can be controlled with low-cost and portable electrochemical readers, which would facilitate a patient's use in the comfort of their own residence, are aspects of future research.

CRediT authorship contribution statement

Manar M. Elhassan: Formal analysis, Investigation, Writing – original draft, Writing – review & editing. **Dalton L. Glasco:** Formal analysis, Investigation, Validation, Writing – review & editing. **Anjaiah Sheelam:** Investigation. **Amr M. Mahmoud:** Writing – review & editing. **Maha A. Hegazy:** Writing – review & editing. **Shereen Mowaka:** Writing – review & editing. **Jeffrey G. Bell:** Conceptualization, Funding acquisition, Methodology, Project administration, Resources, Supervision, Validation, Writing – review & editing.

Declaration of competing interest

The authors declare that they have no known competing financial interests or personal relationships that could have appeared to influence the work reported in this paper.

Data availability

Data will be made available on request.

Acknowledgements

Appendix A. Supplementary data

Supplementary data to this article can be found online at https://doi.org/10.1016/j.bios.2023.115971.

References

Bell, J.G., Mousavi, M.P.S., Abd El-Rahman, M.K., 2018. Electrochemical sensing of carbachol in ophthalmic solutions. J. Electrochem. Soc. 165, B835–B839. https://doi.org/10.1149/2.0571816JES/XML.

Bhidayasiri, R., Chaudhuri, K.R., LeWitt, P., Martin, A., Boonpang, K., Van Laar, T., 2015. Effective delivery of apomorphine in the management of Parkinson disease: practical considerations for clinicians and Parkinson nurses. Clin. Neuropharmacol. 38, 89–103. https://doi.org/10.1097/WNF.0000000000000082.

Bobacka, J., 1999. Potential stability of all-solid-state ion-selective electrodes using conducting polymers as ion-to-electron transducers. Anal. Chem. 71, 4932–4937. https://doi.org/10.1021/AC990497Z.

Bolner, A., Barbato, L., Tagliaro, F., Monge, A., Stocchi, F., Nordera, G., 1997. Determination of apomorphine in human plasma by alumina extraction and high-performance liquid chromatography with electrochemical detection. Forensic Sci. Int. 89, 81–91. https://doi.org/10.1016/S0379-0738(97)00117-5.

Buck, R.P., Lindner, E., 1994. Recomendations for nomenclature of ion-selective electrodes (IUPAC recommendations 1994). Pure Appl. Chem. 66, 2527–2536. https://doi.org/10.1351/PAC199466122527/PDF.

Carbone, F., Djamshidian, A., Seppi, K., Poewe, W., 2019. Apomorphine for Parkinson's disease: efficacy and safety of current and new formulations. CNS Drugs 33, 905. https://doi.org/10.1007/S40263-019-00661-Z.

Cheng, H.-L., Sun, I.-W., 2001. Square-wave voltammetric detection of apomorphine on a nafion film modified glassy carbon electrode. Electroanalysis 13, 1544–1546. https://doi.org/10.1002/1521-4109.

Cheng, H.Y., Strope, E., Adams, R.N., 1979. Electrochemical studies of the oxidation pathways of apomorphine. Anal. Chem. 51, 2243–2246. https://doi.org/10.1021/AC50049A042/ASSET/AC50049A042.FP.PNG_V03.

Diment, L.E., Thompson, M.S., Bergmann, J.H.M., 2017. Clinical efficacy and effectiveness of 3D printing: a systematic review. BMJ Open 7. https://doi.org/10.1136/BMJOPEN-2017-016891.

Ding, J., Qin, W., 2020. Recent advances in potentiometric biosensors. TrAC, Trends Anal. Chem. 124, 115803 https://doi.org/10.1016/J.TRAC.2019.115803.

Dong, S., Zhang, L., 2005. RP-HPLC determination of apomorphine hydrochloride and its related substance in sublingual tablets. Chinese Journal of Pharmaceutical Analysis 25, 1266–1268.

Esteban Muñoz, J., Martí, M.J., Marín, C., Tolosa, E., 1997. Long-term treatment with intermittent intranasal or subcutaneous apormorphine in patients with levodopa-related motor fluctuations. Clin. Neuropharmacol. 20, 245–252. https://doi.org/10.1097/00002826-199706000-00009.

Fibbioli, Monia, Bandyopadhyay, K., Liu, S.G., Echegoyen, L., Enger, O., Diederich, F., Bühlmann, P., Pretsch, E., 2000. Redox-active self-assembled monolayers as novel solid contacts for ion-selective electrodes. Chem. Commun. 339–340. https://doi.org/10.1039/A909532B.

Fibbioli, M., Morf, W.E., Badertscher, M., de Rooij, N.F., Pretsch, E., 2000. Potential drifts of solic-contacted ion-selective electrodes due to zero-current ion fluxes through the sensor membrane. Electroanalysis 12, 1286–1292. https://doi.org/10.1002/1521-4109(200011)12:16.

Gaire, S., Kafle, S., Bastakoti, S., Paudel, A., Karki, K., 2021. Continuous subcutaneous apomorphine infusion in advanced Parkinson's disease: a systematic review. Cureus 13. https://doi.org/10.7759/CUREUS.17949.

Gałuszka, A., Migaszewski, Z.M., Konieczka, P., Namieśnik, J., 2012. Analytical Eco-Scale for assessing the greenness of analytical procedures. TrAC, Trends Anal. Chem. 37, 61–72. https://doi.org/10.1016/j.trac.2012.03.013.

Garrido, J.M.P.J., Delerue-Matos, C., Borges, M.F.M., Macedo, T.R.A., Oliveira-Brett, A. M., 2002. Oxidative behaviour of apomorphine and its metabolites. Bioelectrochemistry 55, 113–114. https://doi.org/10.1016/S1567-5394(01)00169-4.

Glasco, D.L., Ho, N.H.B., Mamaril, A.M., Bell, J.G., 2021. 3D printed ion-selective membranes and their translation into point-of-care sensors. Anal. Chem. 93, 15826–15831. https://doi.org/10.1021/ACS.ANALCHEM.1C03762/SUPPL_FILE/AC1C03762_SI_001.PDF.

Glasco, D.L., Sheelam, A., Ho, N.H.B., Mamaril, A.M., King, M., Bell, J.G., 2022. Editors' choice—review—3D printing: an innovative trend in analytical sensing. ECS Sensors Plus 1, 010602. https://doi.org/10.1149/2754-2726/AC5C7A.

Goud, K.Y., Mahato, K., Teymourian, H., Longardner, K., Litvan, I., Wang, J., 2022. Wearable electrochemical microneedle sensing platform for real-time continuous interstitial fluid monitoring of apomorphine: toward Parkinson management. Sensor. Actuator. B Chem. 354, 131234 https://doi.org/10.1016/J.SNB.2021.131234.

Guinovart, T., Hernández-Alonso, D., Adriaenssens, L., Blondeau, P., Rius, F.X., Ballester, P., Andrade, F.J., 2017. Characterization of a new ionophore-based ion-selective electrode for the potentiometric determination of creatinine in urine. Biosens. Bioelectron. 87, 587–592. https://doi.org/10.1016/J.BIOS.2016.08.025.

Hambly, B., Guzinski, M., Pendley, B., Lindner, E., 2020. Evaluation, pitfalls and recommendations for the "water layer test" for solid contact ion-selective electrodes. Electroanalysis 32, 781–791. https://doi.org/10.1002/ELAN.201900637.

Hattori, N., Nomoto, M., Kimura, T., Kikuchi, S., Enomoto, H., Yoshizawa, K., Tamaoka, A., Hatano, T., Murata, M., Hasegawa, K., Tanaka, K., Arahata, Y., Kanda, F., Kashihara, K., Yamamoto, M., Nishikawa, N., Tsuboi, Y., Ohya, Y., 2014. Sustained efficacy of apomorphine in Japanese patients with advanced Parkinson's disease. Parkinsonism Relat. Disorders 20, 819–823. https://doi.org/10.1016/J.PARKRELDIS.2014.04.008.

Ho, N.H.B., Glasco, D.L., Bell, J.G., 2022. Potentiometric analysis of benzalkonium chloride with 3D printed ion-selective membranes. ECS Sensors Plus 1, 020601. https://doi.org/10.1149/2754-2726/AC8438.

Huang, S., Gan, N., Zhang, X., Wu, Y., Shao, Y., Jiang, Z., Wang, Q., 2019. Portable fluoride-selective electrode as signal transducer for sensitive and selective detection of trace antibiotics in complex samples. Biosens. Bioelectron. 128, 113–121. https://doi.org/10.1016/J.BIOS.2018.12.042.

ICH Harmonized Tripartite Guideline, 1996. Validation of Analytical Procedures: Text and Methodology, Q2 (R1), Current Step 4 Version. Parent guidelines on Methodology.

Isaacson, S., Lew, M., Ondo, W., Hubble, J., Clinch, T., Pagan, F., 2017. Apomorphine subcutaneous injection for the management of morning akinesia in Parkinson's disease. Mov Disord Clin Pract 4, 78–83. https://doi.org/10.1002/MDC3.12350.

Jansod, S., Afshar, M.G., Crespo, G.A., Bakker, E., 2016. Phenytoin speciation with potentiometric and chronopotentiometric ion-selective membrane electrodes. Biosens. Bioelectron. 79, 114–120. https://doi.org/10.1016/J.BIOS.2015.12.011.

Karuppaiah, G., Vashist, A., Nair, M., Veerapandian, M., Manickam, P., 2023. Emerging trends in point-of-care biosensing strategies for molecular architectures and antibodies of SARS-CoV-2. Biosens. Bioelectron. X 13, 100324. https://doi.org/10.1016/J.BIOSX.2023.100324.

Katzenschlager, R., Poewe, W., Rascol, O., Trenkwalder, C., Deuschl, G., Chaudhuri, K.R., Henriksen, T., van Laar, T., Spivey, K., Vel, S., Staines, H., Lees, A., 2018. Apomorphine subcutaneous infusion in patients with Parkinson's disease with persistent motor fluctuations (TOLEDO): a multicentre, double-blind, randomised, placebo-controlled trial. Lancet Neurol. 17, 749–759. https://doi.org/10.1016/S1474-4422(18)30239-4.

Kim, Y., Lee, D., Seo, Y., Jung, H.G., Jang, J.W., Park, D., Kim, I., Kim, J., Lee, G., Hwang, K.S., Kim, S.H., Lee, S.W., Lee, J.H., Yoon, D.S., 2023. Caco-2 cell-derived biomimetic electrochemical biosensor for cholera toxin detection. Biosens. Bioelectron. 226, 115105 https://doi.org/10.1016/J.BIOS.2023.115105.

Kouli, A., Torsney, K.M., Kuan, W.-L., 2018. Parkinson's Disease: Etiology, Neuropathology, and Pathogenesis. Parkinson's Disease: Pathogenesis and Clinical Aspects 3–26. https://doi.org/10.15586/CODONPUBLICATIONS.PARKINSONSDISEASE.2018.CH1.

Kumar, G., Prabhu, K.N., 2007. Review of non-reactive and reactive wetting of liquids on surfaces. Adv. Colloid Interface Sci. 133, 61–89. https://doi.org/10.1016/J.CIS.2007.04.009.

Kuoppamäki, M., Korpela, K., Marttila, R., Kaasinen, V., Hartikainen, P., Lyytinen, J., Kaakkola, S., Hänninen, J., Löyttyniemi, E., Kailajärvi, M., Ruokoniemi, P., Ellmén, J., 2009. Comparison of pharmacokinetic profile of levodopa throughout the day between levodopa/carbidopa/entacapone and levodopa/carbidopa when administered four or five times daily. Eur. J. Clin. Pharmacol. 65, 443–455. https://doi.org/10.1007/S00228-009-0622-Y/FIGURES/3.

Liu, Y., Zeng, X., Waterhouse, G.I.N., Jiang, X., Zhang, Z., Yu, L., 2021. Potential stability improvement in Pb2+ ion selective electrodes by applying hydrophobic polyaniline as ion-to-electron transducer. Synth. Met. 281, 116898 https://doi.org/10.1016/J.SYNTHMET.2021.116898.

Lucotti, A., Tommasini, M., Casella, M., Morganti, A., Gramatica, F., Zerbi, G., 2012. TLC–surface enhanced Raman scattering of apomorphine in human plasma. Vib. Spectrosc. 62, 286–291. https://doi.org/10.1016/J.VIBSPEC.2012.07.009.

Luo, H., Chen, L.X., Ge, Q.M., Liu, M., Tao, Z., Zhou, Y.H., Cong, H., 2019. Applications of macrocyclic compounds for electrochemical sensors to improve selectivity and sensitivity. J. Inclusion Phenom. Macrocycl. Chem. https://doi.org/10.1007/s10847-019-00934-6.

Mamaril, A.M., Glasco, D.L., Yepes, F.A.L., Bell, J.G., 2022. Identifying hypocalcemia in dairy cattle by combining 3D printing and paper diagnostics. ECS Sensors Plus 1, 040601. https://doi.org/10.1149/2754-2726/ACA034.

Manson, A.J., Hanagasi, H., Turner, K., Patsalos, P.N., Carey, P., Ratnaraj, N., Lees, A.J., 2001. Intravenous apomorphine therapy in Parkinson's disease: clinical and pharmacokinetic observations. Brain 124, 331–340. https://doi.org/10.1093/BRAIN/124.2.331.

Mhyre, T.R., Boyd, J.T., Hamill, R.W., Maguire-Zeiss, K.A., 2012. Parkinson's disease. Subcell. Biochem. 65, 455. https://doi.org/10.1007/978-94-007-5416-4_16.

Michael, A.M., Mahmoud, A.M., Fahmy, N.M., 2023. Determination of Clomipramine using eco-friendly solid-contact ionophore-doped potentiometric sensor. BMC Chem 17, 1–9. https://doi.org/10.1186/S13065-023-00938-X/FIGURES/6.

Mousavi, M.P.S., Abd El-Rahman, M.K., Mahmoud, A.M., Abdelsalam, R.M., Bühlmann, P., 2018. In situ sensing of the neurotransmitter acetylcholine in a dynamic range of 1 nM to 1 mM. ACS Sens. 3, 2581–2589. https://doi.org/10.1021/ACSSENSORS.8B00950/SUPPL_FILE/SE8B00950_SI_001.PDF.

National Center for Biotechnology Information, 2023. PubChem Compound Summary for CID 6005, Apomorphine [WWW Document], n.d. URL. https://pubchem.ncbi.nlm.nih.gov/compound/Apomorphine, 8.8.23.

Nikolskii, B.P., Materova, E.A., 1985. Solid contact in membrane ion-selective electrodes. Ion-Selective Electrode Rev. 7, 3–39. https://doi.org/10.1016/B978-0-08-034150-7.50005-X.

Ostergaard, L., Werdelin, L., Odin, P., Lindvall, O., Dupont, E., Christensen, P.B., Boisen, E., Jensen, N.B., Ingwersen, S.H., Schmiegelow, M., 1995. Pen injected apomorphine against off phenomena in late Parkinson's disease: a double blind, placebo controlled study. J. Neurol. Neurosurg. Psychiatry 58, 681–687. https://doi.org/10.1136/JNNP.58.6.681.

Pahwa, R., Koller, W.C., Trosch, R.M., Sherry, J.H., 2007. Subcutaneous apomorphine in patients with advanced Parkinson's disease: a dose-escalation study with randomized, double-blind, placebo-controlled crossover evaluation of a single dose. J. Neurol. Sci. 258, 137–143. https://doi.org/10.1016/J.JNS.2007.03.013.

Palmara, G., Frascella, F., Roppolo, I., Chiappone, A., Chiadò, A., 2021. Functional 3D printing: approaches and bioapplications. Biosens. Bioelectron. 175, 112849 https://doi.org/10.1016/J.BIOS.2020.112849.

Park, J.H., Zhou, H., Percival, S.J., Zhang, B., Fan, F.R.F., Bard, A.J., 2013. Open circuit (mixed) potential changes upon contact between different inert electrodes-size and kinetic effects. Anal. Chem. 85, 964–970. https://doi.org/10.1021/AC3025976/ASSET/IMAGES/MEDIUM/AC-2012-025976_0010.GIF.

Pavan Kalyan, B., Kumar, L., 2022. 3D printing: applications in tissue engineering, medical devices, and drug delivery, 2022 AAPS PharmSciTech 23 (4 23), 1–20. https://doi.org/10.1208/S12249-022-02242-8.

Sajid, M., Płotka-Wasylka, J., 2022. Green analytical chemistry metrics: a review. Talanta 238, 123046. https://doi.org/10.1016/J.TALANTA.2021.123046.

Sam, E., Augustijns, P., Verbeke, N., 1994. Stability of apomorphine in plasma and its determination by high-performance liquid chromatography with electrochemical detection. J. Chromatogr. B Biomed. Sci. Appl. 658, 311–317. https://doi.org/10.1016/0378-4347(94)00239-8.

Shrimanker, I., Bhattarai, S., 2023. Electrolytes. [Updated 2023 Apr 23]. in: StatPearls [Internet]. Treasure Island (FL). https://doi.org/10.1016/B978-0-12-410453-2.00004-X. StatPearls Publishing.

Simon, D.K., Tanner, C.M., Brundin, P., 2020. Parkinson disease epidemiology, pathology, genetics and pathophysiology. Clin. Geriatr. Med. 36, 1–12. https://doi.org/10.1016/J.CGER.2019.08.002.

Smith, L.A., Glasscott, M.W., Vannoy, K.J., Dick, J.E., 2020. Enzyme kinetics via open circuit potentiometry. Anal. Chem. 92, 2266–2273. https://doi.org/10.1021/ACS.ANALCHEM.9B04972/SUPPL_FILE/AC9B04972_SI_001.PDF.

Smith, R.V., Humphrey, D.W., 1981. Determination of apomorphine in tablets using high performance liquid chromatography with electrochemical detection. Anal. Lett. 14, 601–613. https://doi.org/10.1080/00032718108055473.

Späth, A., Knig, B., 2010. Molecular recognition of organic ammonium ions in solution using synthetic receptors. Beilstein J. Org. Chem. 6 https://doi.org/10.3762/BJOC.6.32.

Walker, N.L., Roshkolaeva, A.B., Chapoval, A.I., Dick, J.E., 2021. Recent advances in potentiometric biosensing. Curr. Opin. Electrochem. 28 https://doi.org/10.1016/j.coelec.2021.100735.

Yang, W., Hamilton, J.L., Kopil, C., Beck, J.C., Tanner, C.M., Albin, R.L., Ray Dorsey, E., Dahodwala, N., Cintina, I., Hogan, P., Thompson, T., 2020. Current and projected future economic burden of Parkinson's disease in the U.S. NPJ Parkinsons Dis 6. https://doi.org/10.1038/S41531-020-0117-1.

Zanchi, C., Lucotti, A., Tommasini, M., Trusso, S., de Grazia, U., Ciusani, E., Ossi, P.M., 2015. Au nanoparticle-based sensor for apomorphine detection in plasma. Beilstein J. Nanotechnol. 6 (228 6), 2224–2232. https://doi.org/10.3762/BJNANO.6.228.